Journal of Hydroscience and Hydraulic Engineering
Vol. 2, No. 1, April, 1984, pp.15-25.

BENDING OF THE AXIS OF A SURFACE BUOYANT JET OBLIQUELY DISCHARGED ON THE SHORE

By

Nobuyuki Tamai

Professor, Department of Civil Engineering,

University of Tokyo, Tokyo, Japan

and

Masamitsu Arita

Research Associate, Department of Civil and

Structural Engineering, Tokyo Denki University, Saitama, Japan

SYNOPSIS

The axes of buoyant surface jets discharged into a shallow water obliquely against shoreline gradually change the direction and are bent towards the shore by Coanda effect and then again leave the shore due to shear stresses acting on the bottom of the jets.

This paper presents an analytical and experimental study on the basic features of a surface buoyant jet in the near shore zone. Field observations are also utilized to check the validity of the theory and the labolatory experiments. The physical mechanism of shore entrapment and motion of the surface buoyant jet obliquely discharged onto a sloping beach in a far field is clarified.

INTRODUCTION

Surface buoyant jets from power plants obliquely discharged into a shallow water on the shore with high densimetric Froude numbers, F_{do}, frequently encounter the bending of the axis, which results in the shore entrapment of heated water mass.

Figure 1 shows a typical example of temperature distribution observed off Fukushima coast. Excess temperature is caused by the waste heat disposal from the 5th unit of Fukushima No.1 nuclear power plant. Design criteria of this unit are as follows; the capacity: 784Mw, the maximum discharge: 25.1m^3/sec, the maximum temperature rise: 8.4°c, the width of the outlet: 11.4m, and inclination of the outlet to the shore: 45°. The densimetric Froude number at the outlet, F_{do} is estimated as F_{do}=22. Temperatures of the discharged water and the ambient water are assumed 18°c and 10°c, respectively. Water depth at the outlet is 1.5m. The densimetric Froude number at the outlet of this unit belongs to a relatively higer case.

Behavior of the jet shown in Fig. 1 is classified into two patterns. Pattern I represents the near-field characteristics and jet tends to reattach to the shore. Pattern II represents the far-field characteristics and jet begins to move offshore again.

In this paper, an analysis on the reattachment is performed on an induced velocity field in the ambient water due to entrainment. Hydrauric experiments are also performed to check reproducibility of this type of phenomenon in a distored model and to find out the effects of boundary conditions on the reattachment. The mechanism with which the trapped jet begins to move toward offshore direction

is discussed on the basis of experimental results.

A part of this paper was published by the authors in Japanese paper (6).

ANALYSIS OF THE ENTRAINMENT VELOCITY FIELD IN A NEAR FIELD

Inviscid theory for the flow field

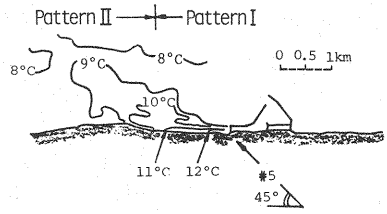

Fig. 1 Representative sample of field data showing the bending of jet axis (Fukushima No. 1 Nuclear Power Station)

Here, a case in which the original inclination of a jet at the outlet is 45° is treated. Fluid is assumed inviscid and the flow fields of both side of the jet axis are called Region I and Region II, respectively as shown in Fig. 2.

For simplicity of the analysis, it is assumed that non-buoyant jet is discharged into a two-dimensional semi-infinite flow field with 45° outlet angle. The entrainment velocity field is simulated by a series of sinks distributed on the jet axis. The magnitude of sinks is assumed to follow a (-1/2)-power of the distance from the outlet. This power law is introduced based on the reduction rate of the velocity along the jet axis and the empirical fact that the entrainment velocity is proportional to the centerline velocity in case of a non-buoyant plane jet. The effect of a boundary wall is taken into consideration by adding virtual sinks of the same magnitude at the positions of mirror image.

The coordinate axis s is taken along the jet axis and n-axis is taken parpendicular to s (See Fig. 2). Notations used in this paper are explained either where they first appear or in Appendix-Notation.

Two individual sinks of strength of $\alpha_1\eta^{-1/2}$ are placed at the points $(0,\eta)$ and $(\eta,0)$ which constitute mirror image concerning the shoreline (See Fig. 3). In such case, a stream function at the points of (s,n) induced by these sinks is explained as follows.

$$\psi_i(s,n) = -\alpha_1\eta^{-1/2}\theta' - \alpha_1\eta^{-1/2}(\pi/2 - \theta'')$$

$$= -\alpha_1\eta^{-1/2}\tan^{-1}\frac{n-\eta}{s} - \alpha_1\eta^{-1/2}\left(\pi/2 - \tan^{-1}\frac{n-\eta}{s}\right) \qquad (1)$$

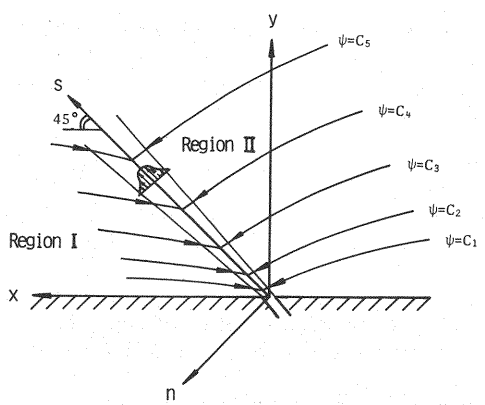

Fig. 2 Schematic diagram of two sinks situated symmetrically to the shoreline

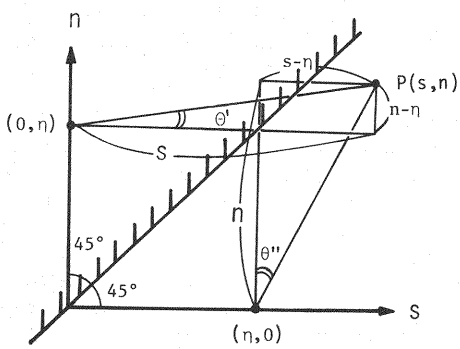

Fig. 3 Coordinate system and division of flow field

Therefore, the stream function Ψ in case of continuosly distributed sinks on the jet axis is explained by the integration of Eq. 1.

$$\Psi(s,n) = \sum \psi_i(s,n)$$
$$= \int_0^\infty \{-\alpha_1 \eta^{-1/2} \tan^{-1} \frac{n-\eta}{s} - \alpha_1 \eta^{-1/2} (\pi/2 - \tan^{-1} \frac{n-\eta}{n})\} d\eta \quad (2)$$

The results of integration for the Region where s>0 and n>0 (Region I) under the condition that $\Psi(s,n)=0$ along a fixed wall is given as follows:

$$\Psi(s,n) = \sqrt{2}\pi\alpha_1 (((s^2+n^2)^{1/2}+s)^{1/2} - ((s^2+n^2)^{1/2}+n)^{1/2})) \quad (3)$$

The value on the s-axis is given by

$$\Psi(s,0) = \sqrt{2}\ (\sqrt{2} - 1)\pi\alpha_1 s^{1/2} \quad (4)$$

From Eq. 4, it is clear that the value of the stream function on the s-axis increases according to the square root of s. Similarly, the stream function for Region II is obtained and final solutions for both regions are summarized as follows:

$$\Psi(s,n) = \begin{cases} \sqrt{2}\alpha_1\pi(((s^2+n^2)^{1/2}+s)^{1/2} - ((s^2+n^2)^{1/2}+n)^{1/2}) & \text{for } s\geq 0, n\geq 0 \\ -\sqrt{2}\alpha_2\pi(((s^2+n^2)^{1/2}+n)^{1/2} - ((s^2+n^2)^{1/2}+s)^{1/2}) & \text{for } s\geq 0, n\leq 0 \\ \sqrt{2}\alpha_2\pi(((s^2+n^2)^{1/2}+s)^{1/2} - ((s^2+n^2)^{1/2}+n)^{1/2}) & \text{for } s\leq 0, n\leq 0 \end{cases} \quad (5)$$

The variation of the velocity along the jet axis in a two-dimensional non-buoyant jet is obtained experimentally by one of the authors(unpublished) as in Eq. 6.

$$\frac{u_c}{u_o} = \left(\frac{1}{5}\ \frac{s}{B}\right)^{-1/2} \quad (6)$$

Coefficients α_1 and α_2 involved in Eq. 5 are determined in the following way. At first the n-component of velocity should coincide on the jet axis computed separately for Region I and II. This is realized in Eq. 7. Then, in Eq. 8 it is realized that the lateral component of the entrainment velocity on the axis is correlated by the longitudinal velocity utilizing Eq. 6.

$$\frac{\partial\Psi(s,0)}{\partial s} = \frac{\sqrt{2}(\sqrt{2}-1)}{2}\pi\alpha_1 s^{-1/2} = \frac{\sqrt{2}(\sqrt{2}+1)}{2}\pi\alpha_2 s^{-1/2} \quad (7)$$

$$\frac{\partial\Psi(s,0)}{\partial s} = v = \alpha_h u_c = \alpha_h u_o \sqrt{5B}\ s^{-1/2} \quad (8)$$

From Eqs. 7 and 8, α_1 and α_2 are given as follows:

$$\alpha_1 = \frac{2\alpha_h u_c \sqrt{5B}}{\sqrt{2}(\sqrt{2}-1)}, \quad \alpha_2 = \frac{2\alpha_h u_c \sqrt{5B}}{\sqrt{2}(\sqrt{2}+1)} \quad (9)$$

Pressure difference between the jet region and the ambient water

Absolute value of the entrainment velocity vector, q is derived from v and an incident angle ϕ of each entrainment velocity vector against jet axis. The relational eqation are shown as follows:

$$q = v/\sin\phi$$
$$v = \alpha_h u_o \sqrt{5B}\ s^{-1/2} \qquad (10)$$

The entrainment velocities of two regions are different because the value of ϕ are different in each region.

The pressure difference between two regions of both sides of the jet is obtained by using Bernoulli eqation. Bernoulli equation applied to Region I and II is as follows:

$$\frac{q_1^2}{2g} + H_1 = \frac{q_2^2}{2g} + (H_1 + \Delta H) \qquad (11)$$

where, suffixes 1 and 2 designate the quantities in Region I and II, and ΔH=difference of water depth in two regions (See Fig. 4). So, the difference of water depth and pressure between two regions are given by the following equations.

$$\Delta H = \frac{(q_1^2 - q_2^2)}{2g} \qquad (12)$$

$$\Delta P \simeq -\rho_a g \Delta H H \qquad (13)$$

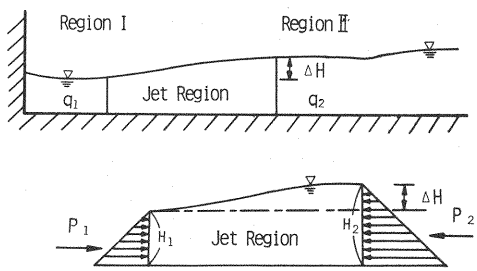

Fig. 4 Difference of water depth and pressure at both sides of jets

Basic equation for bending of the jet axis

In order to explain the bending of the jet axis we have to clarify the forces which exert in the perpendicular direction to the jet. The momentum equation in the n-direction is given as follows:

$$\frac{\partial uv}{\partial s} + \frac{\partial v^2}{\partial n} + \frac{\partial vw}{\partial z} - u^2\frac{\partial \Theta}{\partial s} = -\frac{1}{\rho_a}\frac{\partial p}{\partial n} - \frac{\partial \overline{u'v'}}{\partial s} - \frac{\partial \overline{v'^2}}{\partial n} - \frac{\partial \overline{v'w'}}{\partial z} \qquad (14)$$

Now if we assume $p = \rho_a g z - \overline{w'^2}$, w=0, u=0 and the Reynolds stresses are negligibly small, basic equation is rewritten as follows:

$$\frac{\partial uv}{\partial s} + \frac{\partial v^2}{\partial n} - u^2\frac{\partial \Theta}{\partial s} = -\frac{1}{\rho_a}\frac{\partial}{\partial n}(\rho_a g z) \qquad (15)$$

Integrating Eq. 15 over the jet region ($0 \leqq z \leqq H_1$, $-b \leqq n \leqq b$) and considering that the longitudinal velocity vanishes at the edge of the jet. we obtain a following equation.

$$M(s)\frac{\partial\Theta(s)}{\partial s} = \int_0^{H_1}(v^2_{n=b} - v^2_{n=-b})dz + \frac{1}{\rho_a}\int_0^{H_1}(p_{n=b} - p_{n=-b})dz \qquad (16)$$

where suffix n=b or n=-b designate the value of the quantities at the edge of the jet.

The first two terms in the right hand side of Eq. 16 cancel out to zero because flow rate of entrainment of both side is assumed the same in this analysis. Substituting Eq. 13 into Eq. 16, we obtain Eq. 17.

$$\frac{\partial\Theta(s)}{\partial s} = \frac{1}{M(s)}(g\Delta H H_1) \qquad (17)$$

Momentum flux of the jet is assumed to be conserved and non-dimensional parameter $s_r=s/B$ is introduced. Then, Eq. 17 is rewritten as follows ,to explain the spatial variation of the direction of the jet axis.

$$\frac{\partial\Theta(s_r)}{\partial s_r} = -\frac{gB}{u_0^2}\frac{\Delta H}{B} \qquad (18)$$

EXPERIMENTAL PROCEDURES IN THREE- AND TWO-DIMENSIONAL MODELS

Three-dimensional distorted model

Experiments using a distorted hydraulic model (horizontal scale 1/1500, vertical scale 1/300) is conducted for simulating the thermal diffusion from 5th unit of Fukushima No. 1 nuclear power station. The area covered by the model is 10 km parallel to the shoreline by 3 km perpendicular to it. Bottom slope of the hydraulic model is set equal to 1/20 from the survey of the bottom of the sea.

If the same density defficiency of thermal discharge as that observed in the prototype is used in the experiments, the discharge rate from the outlet of a distorted hydraulic model is given as follows:

$$Q_m = \left(\frac{h_{om}}{h_{op}}\right)^{3/2}\left(\frac{B_m}{B_p}\right)Q_p \qquad (19)$$

Hydraulic model experiment for the basic study on reattachment

Hydrauric model experiments were performed to clarify the effects of boundary conditions on the reattachment. Considered factors are as follows: i) discharge angle of the jet to the water body, Θ_0, ii) densimetric Froude number at the outlet, F_{do}, iii) water depth at the face of the outlet, H_b, and iv) bottom slope of the sea, I. Items i) and ii) were studied in a two-dimensional scheme. Since the experiment was planned to study the fundamental behaviors of the jet and analysis was done on the basis of inviscid fluids, a homogeneous, non-buoyant jet was used in this experiment.

Experiments were conducted in a 1.5m-long, 3m-wide, and 6cm-deep tank. The outlet was 0.5cm wide and constructed at the middle of the tank width. Representative outlet water depth was 3cm and the range of the discharge was 6ml/sec to 45ml/sec. For the nearly critical conditions for reattachment,

reattaching process seemed unstable, which means that under the same experimental conditions the reattachment was observed in some cases and was not in other cases. To be able to observe an essential nature even around the critical condition, a circular plate was inserted for about 1 minute to stabilize the phenomena when the trajectory of jets was uncertain case by case.

CONSIDERATION ON THE BENDING OF PATTERN I

Reproducibility of a distorted hydraulic model

Field data were observed at the site of the 5th unit of Fukushima No. 1 nuclear power plant (1) and experiments were performed for the same magnitude of the densimetric Froude number. A typical exsample of the temperature distribution at the water surface obtained in the experiment is shown in Fig. 5.

The two characteristic patterns of the jet classified into pattern I and II are recoginized and they are similar at least qualitatively to those observed in the prototype and shown in Fig. 1. But the flow pattern in Fig. 5 is not completely similar to that of the prototype because the shear stresses acting on the bottom of the jet cannot be rigorously reproduced due to the restriction of a distorted hydrauric model.

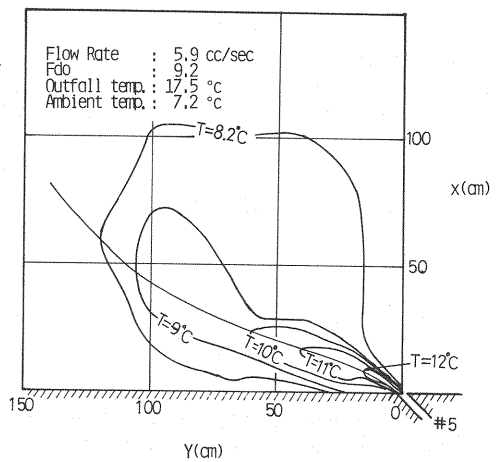

Fig. 5 Experimental result of temperature at the water surface

Bending of the jet axis for a starting buoyant jet in a distorted model

The experimental conditions and horizontal entrainment coefficient (α_h= 0.05) are substituted into Eq. 12 utilizing Eq. 10. Then we obtain the following equation.

$$\frac{\Delta H}{B} = 0.012\left(\frac{s}{B}\right)^{-1} \qquad (20)$$

Equation 20 is substituted to Eq. 18 and is integrated to produce the expression for the variation of the direction of the jet axis with the distance from the origin.

$$\Theta(s_r) = \Theta_o - 0.058 \log s_r \qquad (21)$$

where, Θ_o=discharge angle of the jet to the water body (=45°).

Table 1 Sample calculations about the bending of the jet axis

Sr=S/B	Θ(degree)	S(cm)	Sr=S/B	Θ(degree)	S(cm)
0	45.0°	0	10	37.3°	7.50
1	45.0°	0.75	20	35.0°	15.0
2	42.7°	1.50	100	29.6°	75.0
5	39.6°	3.75	200	25.0°	300.0

H=0.65cm , B=0.75cm , u_o=12.3cm/sec

The calculated result according to Eq. 21 is tabulated in Table 1. It is shown that the rate of bending is about 5° at s_r=s/B=5 (s=3.8cm) and about 10° at sr=s/B=20 (s=15cm). The deflection angle of the jet axis is clearly very small in comparison with experimental results (See Fig. 5).

This discrepancy between the theory and experiment, however, is quite natural The theory is established for sinks distributed on a fixed, straight line along the original direction of discharge. On the other hand, when the jet axis begins to bend toward the shoreline in actual situation by the pressure difference, the pressure difference will be accelerated due to the higher entrainment velocity near the shore side of the jet axis produced by the convergence of stream lines. Therefore, the deflection angle of the jet axis increases in an accelerated manner after the bending starts once.

The progress of bending of the jet axis with lapse of time is shown in Fig. 6 and 7. These figures were obtained for the minimum and the maximum discharge in the experiment. It is seen that the bending of the axis becomes larger and larger as the time elapses after the release. It is considered that the experimental results infer the accelerated process of the bending stated above.

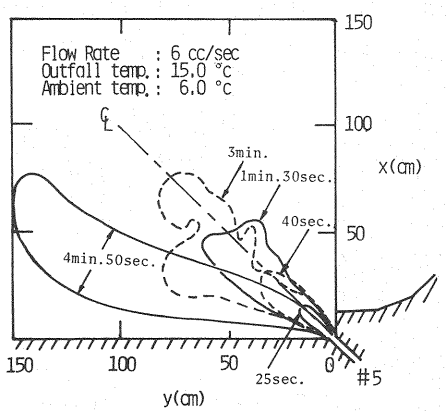

Fig. 6 Experimental results about the process of bending of jet axis (discharge rate ≒ 6ml/sec)

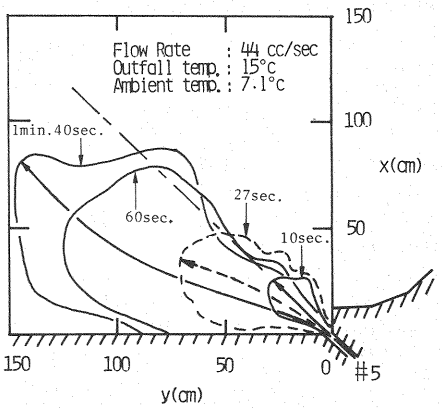

Fig. 7 Experimental results about the process of bending of jet axis (discharge rate = 44ml/sec)

Criteria of the reattachment in a steady state

The important results obtained in two- and three-dimensional experiments are summarized under the four categories.

(a) Eeffect of the discharge angle at the outlet

It is considered the discharge angle at the outlet are most important for the reattachment phenomena. In Fig. 8 previously published data and the experimental results of the present study are summarized. These are theoretical result by Sawyer (4), experimental results by authors, experimental data by Bourque (2), field data of Fukushima No. 1 nuclear power plant (1), and measured at Point-Beach nuclear power station (3). Isotherms on the water surface in Lake Michigan is shown in Fig. 9 (conditions of the outfall and ambient water are listed in the figure). Experimental study by Bourque et al. and theoretical study by Sawyer are conducted to check the Coanda effect in a two-dimentional case. And a part of experimental results by Bourque et al. are eliminated because of the difference in downstream conditions.

The agreement among all data refferred is good and the critical angle for the occurrence of reattachment is recognized

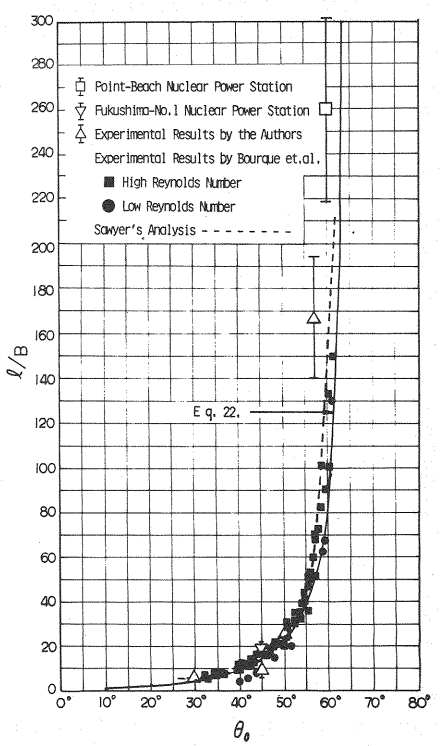

Fig. 8 Relationship between the angle of outlet and the distance of reattachment points

about 64° in the discharge angle. This indicates that the reattachment phenomenon is universally caused by Coanda effect and the direction of the analysis developed in this paper is correct.

The functional form between the distance to the reattachment point ℓ and the discharge angle is derived as the vest fit curve for all the data shown in Fig. 8.

$$\frac{\ell}{B} = \frac{400}{(64 - \Theta_o)} - 6.25 \qquad (22)$$

where Θ_o is explained in degree.

The agreement of field data with Eq. 22 infers that Eq. 22 is applicable even to three-dimentional discharges of buoyant jets, if they are released into a shallow sloping beach. It is noted, however, that the distance to the reattachment point tends to increase near the critical angle for three-dimensional buoyant jets.

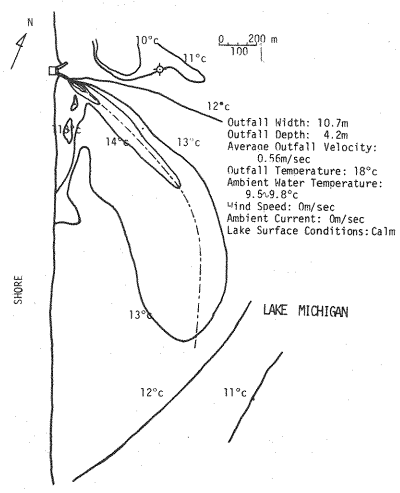

Fig. 9 Representative sample of field-data showing the curvature of jet axis (Point-Beach Nuclear Power Station)

(b) The effect of the densimetric Froude number

The outer boundary of the isotherm of the relative temperature rise of 0.2 (T/T_o=0.2) for various values of F_{do} is shown in Fig. 10. It is seen that the larger the F_{do} is, the stronger the tendency of reattachment is. Especially, in the case that F_{do} is less than 4 the spreading of the isotherm toward the offshore is very large. It is indicated that the process of reattachment may change in the range of low F_{do}, namely $F_{do}<4$. In this range of low F_{do} wide lateral spreading of the high temperature zone may reduce the effective pressure difference between the confined entrainment vortex region (Region I) and outside free entrainment Region (Region II).

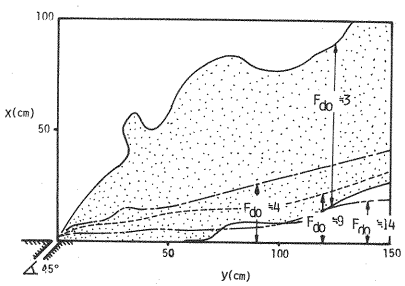

Fig. 10 Outline of Surface Spreading

(c) The effect of the water depth at the face of the outlet

Definition of water depth at the face of outlet H_b is shown in Fig. 11. If H_b is large enough, the horizontally entrained water of Region I is supplied from Region II, too. This conpensating flow will pass under the buoyant jet to reduce the pressure difference between two regions.

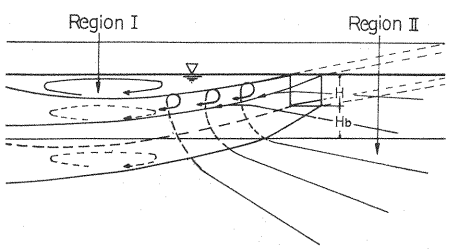

Fig. 11 Schematic diagram of flow field in the case of H_b is large

Experimental results for the discharge angle of 45° are shown in Fig. 12. It is seen that as a value of H_b/H increases, the distance to the reattachment point along the shore rapidly increases. The case of H_b/H=0 corresponds to a two-dimensional experiment. The effect of H_b on the reattachment length is summerized as in the following equation determining the optimum value of coefficients for experimental data.

$$\frac{\ell}{B} = 140 \left(\frac{H_b}{H}\right)^{1.7} + 10 \qquad (\Theta_o = 45°) \qquad (23)$$

(d) The effect of bottom slope

A series of experiments was performed to study the effect of bottom slope on the distance to the reattachment point under the condition that $\Theta_o=45°$ and $H_b=0$. Hydrauric conditions except the bottom slope were kept constant through this series of experiment. Experimental results shown in Fig. 13 explains that the reattachment distance increases linearly with the slope of the beach. The average value in experiments is explained as follows:

$$\frac{\ell}{B} = 470\ I + 10 \quad (\ \Theta_o=45°\ ) \tag{23}$$

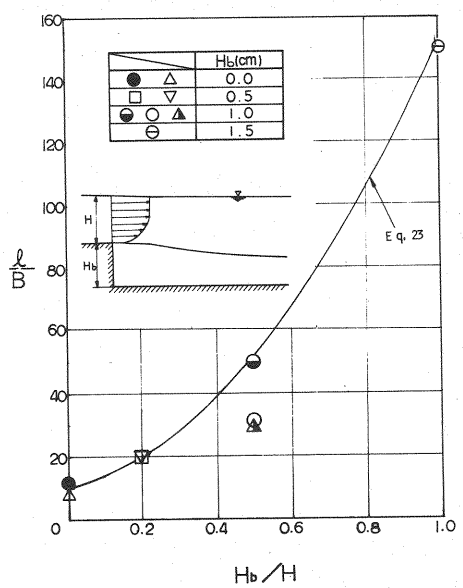

Fig. 12 Distance of reattachment points corresponding to various value of Hb (discharge angle = 45°; The full line shows Eq. 23.)

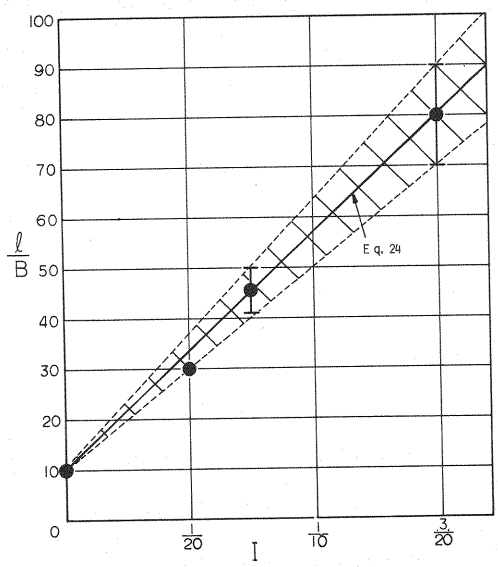

Fig. 13 Distance of reattachment points corresponding to various bottom slope (discharge angle = 45° ; The full line shows Eq. 24.)

COSIDERATION ON THE BENDIG OF PATTERN II

In this chapter the flow behavior in the far-field where the jet begins to move offshore again is discussed.

Komori et al. (4) observed the similar phenomenon in the thermal discharge from the No. 1 unit of Fukushima nuclear power plant. In case of the No. 1 unit the waste heat is discharged southward and parallel to the shoreline. They reported that the cause of this offshore movement of the jet is unbalance of shear stress which exerts the bottom of the jet. In the shoreline side of the jet the depth of water is shallower and the shear stress on the bottom is larger than that of the offshore side. Consequently, the jet flowing parallel to the shore tends to move offshore where the resistance to the jet is small.

The bending of Pattern II in this study may be induced by the same mechanism as that reported by Komori et al. To prove this hypothesis, experiments were conducted in case of deep water and a two-dimensional model. In such cases, the tendency of the jet axis to leave the shore in the far-field was found less clearly. Accordingly, the explanation based on the unbalance of shear exerting on the bottom of the jet region is cinsidered correct and acceptable.

CONCLUSIONS

1) An analytical model to explain the bending of the surface buoyant jet discharged obliquely into a shallow water is presented based on the difference of the entrainment velocity fields of both sides of the jet. Consideration on the unsteady effect in case of a starting buoyant jet is a further subject in future.

2) Reattachment in the near field and motion toward offshore in the far-field are reproducible in a small distorted hydraulic model, the distortion rate of which is five.

3) It is inferred that the reattachment of thermal discharge is also caused by the Coanda effect and critical discharge angle is about 64° in summarizing previous experimental and field data.

4) Influences of various components on the distance to the reattachment point are clarified experimentally. Decrease of the outlet densimetric Froude number, increase of the water depth at the face of the outlet, and increase of the beach slope cause the tendency of reattachment week.

5) The bending of the jet axis toward offshore in the far field is explained due to unbalance of shear exerting on the bottom of the jet region.

REFERENCES

1. Administration comittee of Fukushima Prefecture for thermal discharges: Reports about the investigations of thermal discharges in 1974.∿ Reports about the investigations of thermal discharges in 1978.
2. Bourque,C. and B.G. Newman : Reattachment of a two-dimentional imcompressible jet to an adjacent flat plate, Aer. Quart., Vol.11, pp.201-232, 1960.
3. Frigo, A.A. and D.E. Frye : Pysical measurements of thermal discharges into Lake Michigan, ANL Report, No. ANL/ES-16, 1972.
4. Komori, K.S., T. Tanaka and A. Wada : Experimental study on thermal dispersion in and near the surf zone, CRIETI Report No. 377018, June, 1978.
5. Sawyer R.A. : Two-dimensional reattaching jet flows including the effect of curvature on entrainment, JFM, Vol.17, pp.481-498, 1963.
6. Tamai, N. and M. Arita : Bending of the axis of an obliquely discharged surface buoyant jet, Proc. 29th Conf. on Coastal Eng. in Japan, pp.535-539, 1982(in Japanese).
7. Taylor, G.I. : Flow induced by jets, JASS, pp.464-465, July, 1958.

APPENDIX - NOTATION

The following symbols are used in this paper:

B = outlet width;

b = width of the plume;

B_m, B_p = outlet width of distorted hydraulic model and prototype;

F_{do} = outfall densimetric Froude number;

g = acceleration of gravity;

h_{om}, h_{op} = outlet depth of distorted hydrauric model and prototype;

H = outlet depth;

H_1 = water depth of Region I;

H_b = water depth at the face of outlet;

ΔH = difference of water depth between Region I and II;

ℓ = distance from outlet to the reattachment points;

$M(s)$ = momentum flux of jet;

n = horizontal coordinate which is perpendicular to s;

p = pressure of water;

P_1, P_2 = pressure force exerting to Region I and II;

ΔP = difference of pressure force between Region I and II;

q = absolute value of entrainment velocity;

q_1, q_2 = components of Region I and II

Q_m, Q_p = flow rate of distorted hydraulic model and prototype;

s = coordinate along jet trajectory;

s_r = non-dimensional parameter of s (s_r=s/B);

T = temperature of water;

ΔT_c = temperature rise of jet trajectories;

T_o = outlet temperature rise;

u_o = outlet velocity;

u, v, w = s, n, z component of velocity;

u', v', w' = velocity fluctuations of u, v, w;

u_c = the value of u along the centerline;

α_1, α_2 = constants for magnitude of sinks in Region I and II, respectively;

α_h = horizontal entrainment coefficient;

η = distance to sink from the origin on s and n axes;

Θ' = angle between the s-axis and a line which passes througth the point (s,n) and a sink on the n-axis;

Θ'' = angle between the n-axis and a line which passes through the point (s,n) and a sink on the s-axis;

Θ_o = angle of the jet axis at outlet;

$\Theta(s)$ = angle of the jet axis;

ρ = density of water;

ρ_a = density of ambient water;

ϕ = incident angle against jet axis of entrainment; and

ψ_i, Ψ = stream functions, respectively.